Atomistic simulation of track formation by energetic recoils in zircon

2010 J. Phys.: Condens. Matter 22 395008

(http://iopscience.iop.org/0953-8984/22/39/395008)

J. Phys.: Condens. Matter **22** (2010) 395008 (9pp) doi:10.1088/0953-8984/22/39/395008

Atomistic simulation of track formation by energetic recoils in zircon

Pedro A F P Moreira[1], Ram Devanathan[2,5] and William J Weber[3,4]

[1] Instituto de Fisica 'Gleb Wataghin', Universidade Estadual de Campinas, Campinas, SP, 13083-970, Brazil
[2] Chemical and Materials Sciences Division, Pacific Northwest National Laboratory, MS K2-01, Richland, WA 99352, USA
[3] Department of Materials Science and Engineering, University of Tennessee, Knoxville, TN 37996, USA
[4] Materials Science and Technology Division, Oak Ridge National Laboratory, Oak Ridge, TN 37831, USA

E-mail: ram.devanathan@pnl.gov

Received 4 July 2010, in final form 30 August 2010
Published 17 September 2010
Online at stacks.iop.org/JPhysCM/22/395008

Abstract
We have performed classical molecular dynamics simulations of fission track formation in zircon. We simulated the passage of a swift heavy ion through crystalline zircon using cylindrical thermal spikes with energy deposition (dE/dx) of 2.5–12.8 keV nm^{-1} and a radius of 3 nm. At a low dE/dx of 2.55 keV nm^{-1}, the structural damage recovered almost completely and a damage track was not produced. At higher values of dE/dx, tracks were observed and the radius of the track increased with increasing dE/dx. Our structural analysis shows amorphization in the core of the track and phase separation into Si-rich regions near the center of the track and Zr-rich regions near the periphery. These simulations establish a threshold dE/dx for fission track formation in zircon that is relevant to thermochronology and nuclear waste immobilization.

(Some figures in this article are in colour only in the electronic version)

1. Introduction

Zircon ($ZrSiO_4$) has been proposed as a host material for the immobilization of high-level nuclear waste and plutonium [1]. It is a chemically and mechanically durable mineral that is widely distributed in the earth's crust. It occurs in nature with U and Th concentrations ranging from ppm to a few wt% [1]. Fission tracks in zircon are used in geothermochronology to understand the thermal history of the continental crust. A common feature of fission fragments in natural minerals and swift heavy ions (SHIs) in laboratory irradiation experiments is that they leave a trail of highly disordered atoms in a crystalline material as a result of electronic energy loss processes. These tracks can be etched, imaged and counted. By combining zircon fission track analysis with U–Pb dating in a novel analytical approach called double-dating, valuable insights can be obtained into the geologic history of rocks [2]. Since the fission tracks are disordered regions, they can provide rapid migration pathways for Pb in minerals used in radiometric dating and enhanced leaching of actinides in waste forms. This has important implications for both geological-age determination and nuclear waste immobilization. Therefore, it is essential to understand the fundamental mechanisms of track formation and the structure of tracks in irradiated zircon.

Radiation damage produced by energetic recoils in zircon has been extensively studied by experiment [1, 3–6]. These studies have examined damage to the crystalline lattice in natural zircon from U and Th decay, Pu-loaded synthetic zircon from self-radiation, and synthetic zircon following energetic particle irradiation. It is known that synthetic zircons are amorphized by self-radiation from Pu decay and ion irradiation, and natural zircon is converted to the amorphous 'metamict' state by alpha-decay. In the case of α-decay, most of the damage is caused by the α-recoil. However, the radiation effects produced by α-recoils are different from that produced by heavier and more energetic fission fragments. The typical

[5] Author to whom any correspondence should be addressed.

mass of fission fragments is 90–130 amu with energies of about 1 MeV/nucleon [6].

Recently, the formation of fission tracks in natural zircon under crustal conditions has been reproduced under laboratory conditions using relativistic heavy ion irradiation [6]. Fission tracks of about 5 nm diameter were observed. The boundary between the amorphous and crystalline domains could not be clearly defined by electron microscopy, because the sample geometry and track orientation were such that the electron beam passed through both domains. Due to the extreme and transient conditions of track formation, the steps in the evolution of a fission track cannot be currently determined by experimental observation.

Rapid dissipation of the deposited energy can produce amorphous or disordered crystalline regions or a combination of the two depending on the competition between amorphization and recrystallization processes. The mode-coupling theory (MCT) can describe the amorphization process [7, 8]. MCT considers three distinct transport regimes. In the initial stage, atoms move along ballistic paths and the mean square displacement (MSD) of the particles scales proportional to the square of time ($\sim t^2$). At longer times, atomic mobility depends markedly on temperature. A random walk process governs atomic motion in this diffusive regime and the MSD is proportional to t. Between these regimes, a plateau region occurs, where the MSD increases very little with time. A particle in this regime is beyond the ballistic stage, but despite many collisions with other particles it remains confined in a small region of space and does not show diffusive behavior. The length and timescales of these processes are such that molecular dynamics simulations can be used to examine the formation and structure of the disorder induced by the passage of SHIs.

Atomistic simulations have been used previously to study recoil damage in zircon [9–11]. These studies have shown that energetic recoils cause direct impact amorphization and that there is nanoscale phase separation into Zr-rich and Si-rich domains in the radiation-damaged region. These simulations considered only the nuclear stopping process, because current computational resources do not permit rigorous modeling of electronic energy loss processes at energies of about 1 MeV/nucleon. Various approximations have to be invoked to account for the energy transfer to electronic excitations and subsequent rearrangement of lattice atoms. Coulomb explosion [12], thermal spike [13–15] or a combination of the two [16] have been proposed to explain the appearance of tracks induced in matter by the slowing down of energetic ions in the electronic stopping power regime. Itoh *et al* [17] have discussed various models of track formation by SHIs.

In the thermal spike model, the energy deposited by a SHI is transferred to electrons and then to the lattice atoms. The transfer of energy from electronic excitations to the nuclei by electron–phonon coupling can lead to a local thermal spike and pressure waves that cause material modification by driving the system far from equilibrium [13–15]. Recent work has employed a two-temperature model that assigns different temperatures to the electronic and lattice subsystems to study swift heavy ion damage in metals and ceramics [18, 19].

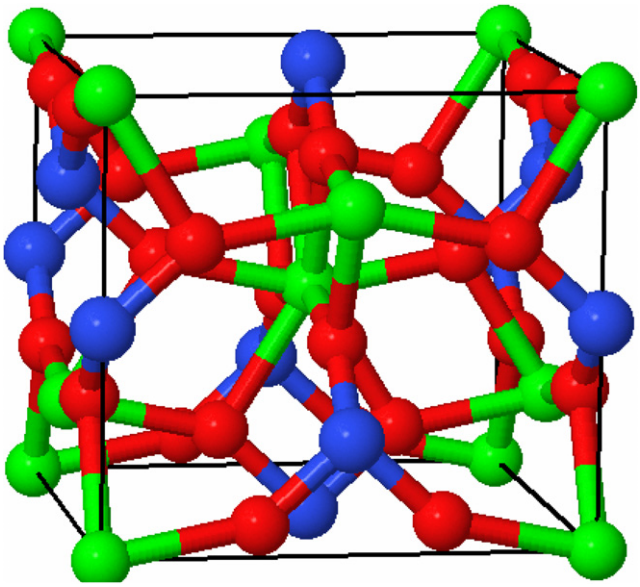

Figure 1. The unit cell of zircon. Zr, Si and O atoms are shown as green, blue and red spheres, respectively.

We have previously used a simple thermal spike model to study the response of magnesium silicate [20] gadolinium titanate [21] and gadolinium zirconate [21] to the passage of swift heavy ions. The results of this simple model have shown remarkable agreement to experimental observations and have shed light on track formation in pyrochlore [21]. In the present work, we have employed the thermal spike model in classical molecular dynamics simulations for five different values of energy deposition per unit length in zircon. The goal of the work is to determine the profiles of the resulting tracks, analyze the number and types of defects produced, and study the energy dependence of the observed phenomena. The present analysis includes a study of MSD that shows that fission track formation in zircon can be described by the MCT.

2. Details of the simulations

For the simulation of thermal spikes, we generated a zircon supercell with 1200 000 atoms arranged in 50 × 50 × 20 unit cells (33.0 × 33.0 × 12.2 nm). This supercell reproduces the zircon crystal structure that is body-centered tetragonal (space group $I4_1/amd$) with four $ZrSiO_4$ formula units per unit cell. The unit cell can be seen in figure 1. The c lattice parameter is shorter than the a lattice parameter. The arrangement of O is such that the structure consists of edge sharing SiO_4 tetrahedra and ZrO_8 dodecahedra. Each Si is coordinated by four O at a bond distance of 0.162 nm, while each Zr is coordinated by four O at 0.213 nm and four O at 0.227 nm as shown by the body-centered atom in figure 1. Each O is bonded to two Zr and one Si. The Si atoms are not networked by common O neighbors, i.e. there is no Si–O–Si polymerization, in perfect crystal $ZrSiO_4$. Starting from this perfect crystal structure, we performed MD simulations using the DL_POLY code [22] developed at Daresbury Laboratory, UK.

Table 1. The values of energy loss per length unit (dE/dx) for the thermal spike simulated in the present work and the corresponding energy per atom.

dE/dx (keV nm^{-1})	Energy per atom (eV/atom)
2.55	1.00
3.90	1.56
5.94	2.33
7.65	3.00
12.75	5.00

The reliability of MD results depends on the fidelity of the potential. We used a recently developed potential that has been shown to be well suited to study the structure and mechanical properties of various phases of $ZrSiO_4$, ZrO_2, and SiO_2 [23]. Using this potential, we have determined the displacement threshold energy for Zr, Si and O to be about 116, 120, 60 eV, respectively in agreement with experimental estimates [24]. The partial-charge, rigid-ion interatomic potential used [23] consists of a Coulombic term and a short-range Buckingham potential. The potential was smoothly joined to the Ziegler–Biersack–Littmark potential [25] by a spline function at close separations to avoid unphysical attraction between ions. The potential parameters, fitting procedure, and the use of a repulsive potential at close separations have been discussed in detail previously [23]. We used periodic boundary conditions and initially equilibrated the simulation cell in the isothermal isobaric ensemble at 300 K and zero external pressure, i.e. constant NPT ensemble with Berendsen barostat and thermostat [26], for 10 ps. Throughout this work, we used a variable time step algorithm with minimum and maximum atomic displacements of 0.003 and 0.01 nm, respectively.

We created thermal spikes for five different values of energy deposition by providing random velocities to ions within a cylinder of 3 nm radius. The cylinder was centered in the X- and Y-dimensions ((100) and (010) directions) and ran along the entire length (12.2 nm) of the cell along the Z-dimension ((001) direction). The velocities of the ions inside this cylinder were chosen based on kinetic energies of 1–5 eV/atom, as listed in table 1. The initial kinetic energy was the same for all ions in the cylinder, but the ions were initiated with velocities in random directions. The corresponding energy deposition per unit track length (dE/dx) varied from 2.55 to 12.75 keV nm^{-1}. This value will be equivalent to the experimentally determined dE/dx value only for the unrealistic case of perfect electron–phonon coupling. In reality, the electron–phonon coupling efficiency is less than 1.0 and the corresponding experimental dE/dx value is higher. For instance, if the electron–phonon coupling efficiency is taken to be 0.3, the corresponding experimental dE/dx varies from 8.5 to 42.5 keV nm^{-1}. A total of 31 126 ions were present in the spike initially, including 5212 $Zr^{2.4+}$, 5215 $Si^{2.4+}$ and 20 699 $O^{1.2-}$.

We performed the thermal spike simulations with the microcanonical (constant NVE) ensemble. The temperature prior to introduction of the spike was 300 K. After the introduction of the thermal spike, the temperature of the simulation cell increased with time and reached a constant value that was as high as 650 K. Each simulation ran for 52 000 variable steps with time steps between 0.01 and 2 fs. The run time was different for each thermal spike, but all the runs were sufficiently long for the number of defects produced to reach steady values. We saved the ion positions and velocities, and forces on the ions at intervals of 1000 steps, subsequently analyzed these trajectories and visualized them using the VMD software [27]. We identified defects based on the coordination environment of ions with cutoff distance of 0.2 and 0.3 nm, respectively, for Si–O and Zr–O bonds. Zr cations with coordination number less than eight, Si cations that are connected to other Si cations by anion bridges, and O anions coordinated by no Si cations or by more than one Si cation are classified as defects in this scheme. A defect is considered to be part of an amorphous region if more than half the neighbors within 0.3 nm are also defects. The set of ions in the amorphous region is a subset of the set of defects. The results provide insights into experimental studies of fission tracks in zircon by showing the intermediate steps in track formation, extent of amorphization and differences in track structure along the track radius.

3. Results and discussion

The excess energy deposited in the thermal spike is dissipated by creation of defects and energy transfer to the surrounding lattice. Figure 2 shows the numbers of defects, ions in amorphous domains and hot ions, i.e. ions with kinetic energies (KE) greater than 1.0 eV, as a function of time for the five different values of dE/dx simulated. It is clear that all simulations were run sufficiently long for the numbers of defects and ions in amorphous clusters to reach steady values and the number of hot ions to decay to zero. For the lowest dE/dx examined (2.55 keV nm^{-1}), the thermal spike did not produce amorphization. Figure 2(a) shows that the damage is completely recovered after 10 ps for dE/dx of 2.55 keV nm^{-1}. At a higher dE/dx of 3.90 keV nm^{-1}, permanent defects and amorphous regions were observed. Therefore, the threshold value of dE/dx for defect production and amorphization in zircon lies between 2.55 and 3.9 keV nm^{-1}. Previous work shows that the threshold dE/dx for amorphization in SiO_2 is below 5 keV nm^{-1} [17]. A recent molecular dynamics simulation in quartz and amorphous SiO_2 has calculated this value to be 3.6 keV nm^{-1} [28]. One can also observe from figure 2 that the time needed for decay of the deposited energy, given by the decrease to zero of the number of ions with KE in excess of 1 eV, increases with increasing dE/dx. Larger simulation cells to facilitate energy dissipation and longer simulation times to reach steady state are needed for dE/dx values much higher than 12.75 keV nm^{-1}.

We have analyzed the spatial distribution of defects and amorphous regions as a function of radial distance from the central axis of the initial cylindrical thermal spike. We calculated the number of defects in a cylinder of radius 0.1 nm and then determined the number of defects in concentric shells of radius increasing by 0.1 nm. Plotting Zr, Si and O defects separately as a function of radial distance and at different times requires a three-dimensional plot. Moreover, since the number

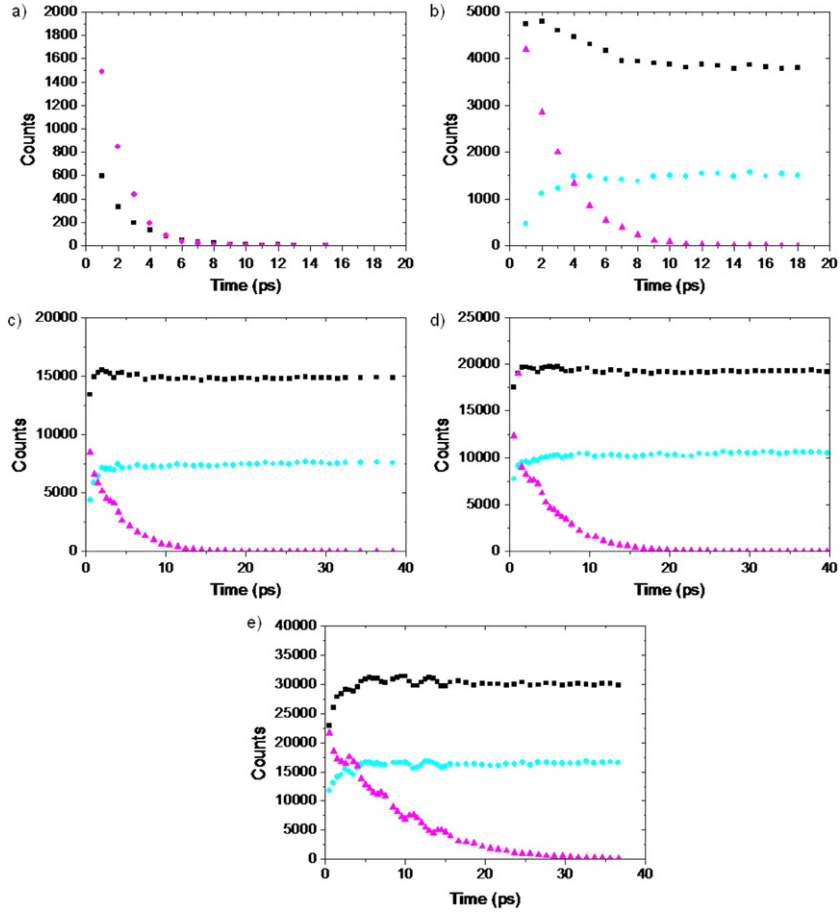

Figure 2. The temporal evolution of the ions with kinetic energy greater than 1 eV (pink triangle), the number of defects (black square), and number of ions in amorphous regions (light blue circle) in thermal spikes for the following dE/dx values. (a) 2.55; (b) 3.90; (c) 5.94; (d) 7.65; (e) 12.75 keV nm^{-1}.

of atoms in the concentric shells increases with increasing radial distance from the axis, dividing by the volume and plotting the density is an efficient method of representing the radial defect profile. We have condensed the defect data in figure 3 by plotting the mass density of defects as a function of radial distance from the center of the track at different times during the thermal spike evolution. Zircon has a mass density of 4.6 g cm^{-3}. Thus, a defect density of 2.3 g cm^{-3} represents 50% of the ions being defects, assuming the local density has not changed appreciably and that the proportion of Zr, Si and O ions in the track is the same as in the perfect crystal. Even if these assumptions are not strictly valid, the calculated defect density profiles give insights into the temporal evolution of the spatial distribution of defects for different levels of energy deposition.

The sharp defect profiles for 0.5 and 1.0 ps indicate the quick response of the lattice to the energy deposited by the thermal spike. The data points closest to the axis are less reliable as fewer ions are sampled and one observes more fluctuations closer to the axis. The radial extent of the damage increases with increasing dE/dx. For dE/dx of 3.90 keV nm^{-1}, only the core of the thermal spike, within a radius of about 1.5 nm, is permanently damaged on these timescales. For dE/dx of 5.94 and 7.65 keV nm^{-1}, the damaged region nearly coincides with the size of the initial thermal spike. At the highest dE/dx examined of 12.75 keV nm^{-1}, the damage extends well beyond the edge of the original thermal spike, showing that the track radius can be smaller or larger than the radius of the cylinder into which energy is deposited. It must be acknowledged that the use of a thermal spike profile with an abrupt edge, i.e. a step function in energy, is an approximation. In future work, we intend to use a diffuse profile. The reason for using a step function is that it is not entirely clear what the shape and width of a diffuse distribution should be.

Based on the radial distribution of defects, three well-defined regions can be identified. The first region, which is closest to the axis and referred to as the primary damage region, is a plateau of high defect density that comprises much of the damage track. The adjacent transition region is where the defect density decays from the high value in the primary damage region to zero. Finally, the undamaged region is the rest of the crystal that has no thermal spike-induced defects but experiences heating and pressure waves. The thermal conductivity of this region will play an important role in the evolution of the primary damage and transition regions. The extent of amorphization in these two regions is shown in figure 4 in the form of plots of the radial distribution of the

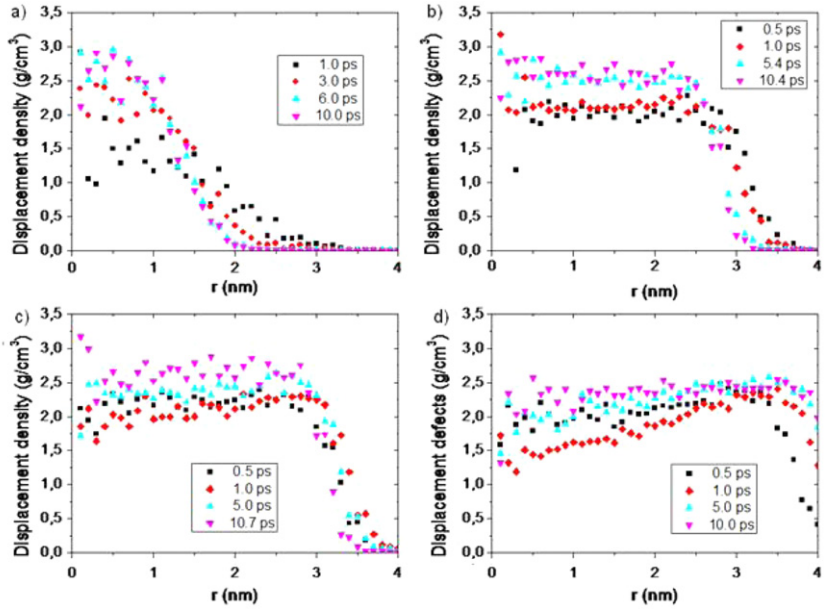

Figure 3. The change in defect density with radial distance, r, in thermal spikes at various times for the following $\mathrm{d}E/\mathrm{d}x$ values: (a) 3.90, (b) 5.94, (c) 7.65, (d) 12.75 keV nm^{-1}.

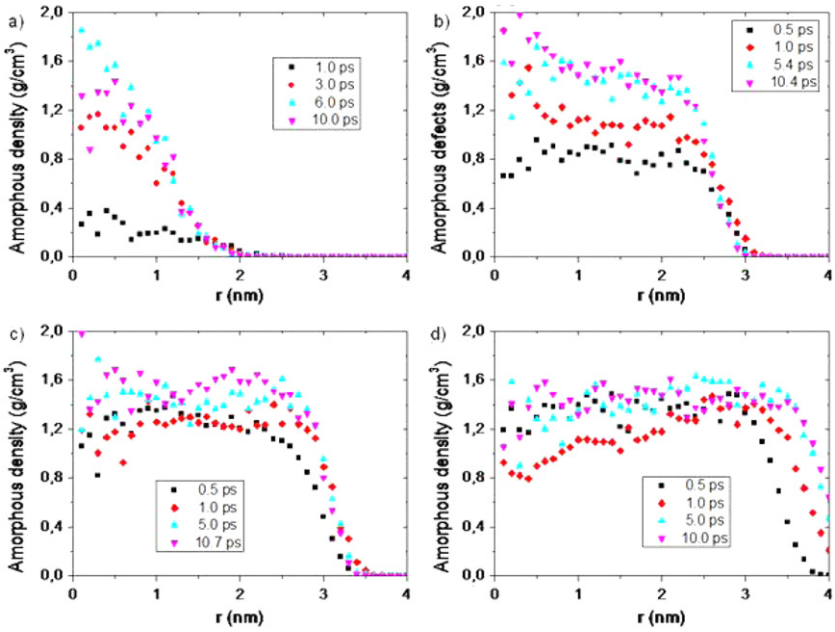

Figure 4. The change in density of amorphous clusters with radial distance, r, in thermal spikes at various times for the following $\mathrm{d}E/\mathrm{d}x$ values: (a) 3.90, (b) 5.94, (c) 7.65, (d) 12.75 keV nm^{-1}.

density of ions in amorphous regions at various times and for different values of $\mathrm{d}E/\mathrm{d}x$. This density is not the density of amorphous zircon but the ratio of the mass of amorphous clusters in a given volume at a certain radius to the volume. If all the ions in a given volume are amorphous, then this value would represent the density of amorphous zircon.

It is interesting to note that the primary damage plateau is absent in figure 4(a) for $\mathrm{d}E/\mathrm{d}x$ of 3.9 keV nm^{-1}. There is minimal amorphization, which indicates that 3.9 keV nm^{-1} may be close to the threshold for track formation. For all values of $\mathrm{d}E/\mathrm{d}x$ shown, the plateau is narrower in figure 4 than in figure 3. Moreover, the transition region starts closer to the axis and is wider in figure 4 than in figure 3. The radius of the amorphous plateau increases with increasing $\mathrm{d}E/\mathrm{d}x$ from zero at 3.9 keV nm^{-1} to 3 nm, i.e. the original thermal spike radius, at 12.75 keV nm^{-1}. By taking the ratio of the distribution shown in figure 4 to that in figure 3 one can obtain the fraction of the damage that is amorphous as a function of space, time and $\mathrm{d}E/\mathrm{d}x$. Thus figures 3 and 4 present a wealth of information about the dynamics of fission track formation in zircon that cannot be directly obtained by experiment and thereby demonstrate the value of computer simulation in the

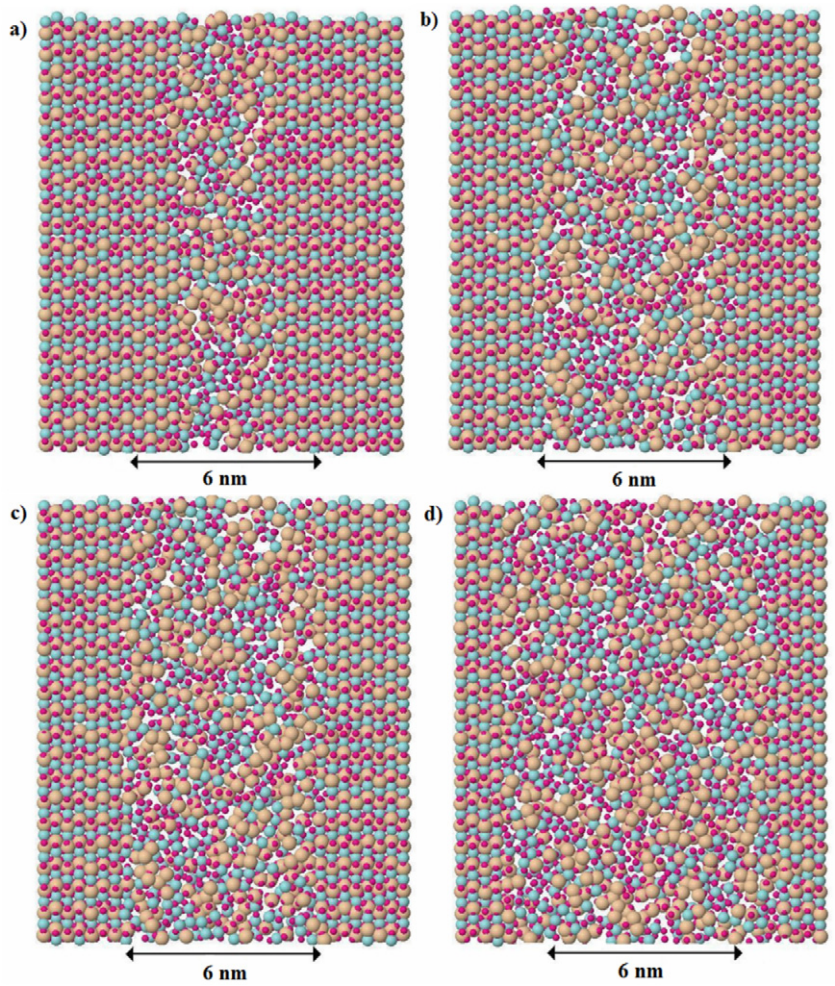

Figure 5. Projection of atom positions in a slice through the center of fission tracks from the final configuration for the following dE/dx values: (a) 3.90; (b) 5.94; (c) 7.65; and (d) 12.75 keV nm^{-1}. Blue circles are Zr, orange ones are Si and red ones are O.

study of radiation damage. We have plotted the defect and amorphous densities up to 10.0 ps, because we did not see any change in the profiles beyond 10 ps.

Mathematical analysis of defect and amorphous clusters, presented in figures 3 and 4, provides a very detailed picture of the track evolution. The same information can be visualized by projecting the atom positions at various stages in the process of track formation. Figure 5 shows two-dimensional projections of atom positions in a slice through the center of the tracks. The track diameter increases with increasing dE/dx from 3.9 to 12.75 keV nm^{-1}. The original spike diameter is indicated at the bottom of the projection. At the highest dE/dx examined, the track diameter extends beyond the extent of the initial spike. The visualization confirms the validity of our mathematical analysis, and also indicates that the density of the track region may be lower than that of the surrounding crystal. Our previous molecular dynamics study using this potential has shown that melt-quenched zircon is 10% less dense than crystalline zircon [23].

In an effort to examine density variations in the fission track, we have calculated the density within a cylinder of radius 0.5 nm at the center of the track and in concentric shells of 0.5 nm thickness. The density variation with radial distance is plotted at various times for dE/dx of 7.65 keV nm^{-1} in figure 6. Within 0.5 ps, the density inside a cylinder of radius 2 nm decreases by 20% relative to the density of crystalline zircon. After 1 ps, the decrease in density in this core region is 28%. The initial pressure wave causes a flow of matter from the center of the track to the surrounding regions. At longer times, the surrounding crystal relaxes and some of the matter flows back to the track core. The density of the core region increases and the final density within a cylinder of radius 3 nm from the center of the original thermal spike reaches a constant value of about 4.3 g cm^{-3}. This is about 6.5% below the value for perfect crystal zircon, but the density is higher than that of melt-quenched zircon. Therefore, it is reasonable to conclude that the center of the track consists of both crystalline and amorphous regions. Similar density variations have been observed in experimental studies of swift heavy ion-irradiated SiO_2 [28].

Our simulations show that for dE/dx values of 3.9 keV nm^{-1} or higher, the fission track in zircon has a core region containing amorphous clusters and defects, surrounded by a shell that is rich in defects but lacks amorphous clusters, which is in turn surrounded by undamaged crystal. This type of core–shell morphology has been observed previously

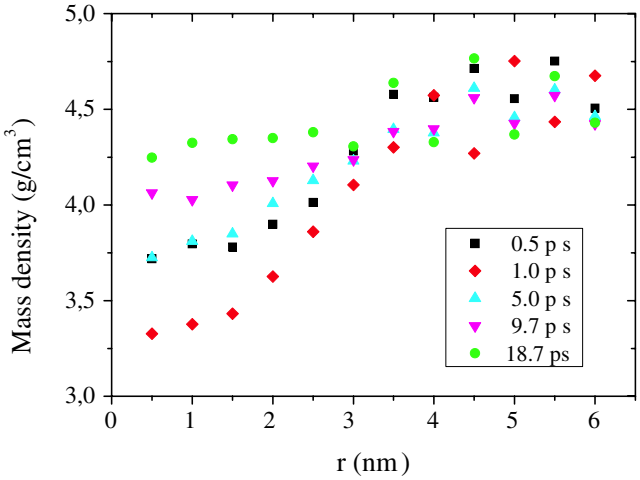

Figure 6. Density variation with radial distance from the axis of the thermal spike for $\mathrm{d}E/\mathrm{d}x$ value of 7.65 keV nm^{-1} at various times during fission track evolution.

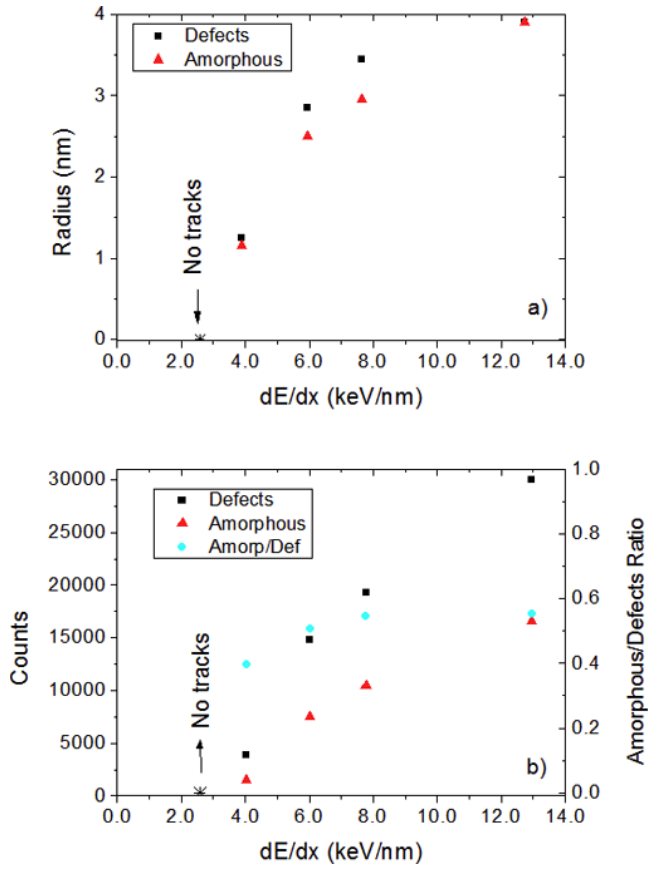

Figure 7. (a) Radius of region containing defects (black squares) and amorphous clusters (red triangles) as a function of $\mathrm{d}E/\mathrm{d}x$.
(b) Counts of defects (black squares) and amorphous clusters (red triangles) as a function of $\mathrm{d}E/\mathrm{d}x$ (use left ordinate) and the ratio of ions in amorphous clusters to defects (light blue circles) as a function of $\mathrm{d}E/\mathrm{d}x$ (use right ordinate). The black asterisk indicates the minimum threshold $\mathrm{d}E/\mathrm{d}x$ for defect and amorphous cluster formation.

in silica [28] and pyrochlore [21]. By taking the ratio of the amorphous density in figure 4 to the material density in figure 6, one can estimate the fraction of ions in the core that are in amorphous clusters. Similarly, by taking the ratio of defect density values in figure 3 to the density in figure 6, one can estimate the defect fraction as a function of radial distance from the track axis. About 40% of the track core consists of amorphous material and about 60% is made up of defects (including amorphous material). Thus about 20% of the core atoms are in defective crystalline regions. Nearly 40% of the core atoms are not defects. This mixture of crystalline, defective and amorphous regions in the track core may change at higher $\mathrm{d}E/\mathrm{d}x$, but it shows that the track core is not completely amorphous. The overlap of tracks may be needed to drive the material to the completely amorphous or metamict state.

Our simulations started with thermal spikes of 3.0 nm radii, but the final damage track radii range from 0 nm up to ∼4 nm, considering only the primary region. The final track radius is not the same as the radius of the initial spike, and it increases with increasing $\mathrm{d}E/\mathrm{d}x$. Figure 7(a) is a plot of two measures of the radius of tracks as a function of $\mathrm{d}E/\mathrm{d}x$. The radius can be calculated by considering the profile of defects (figure 3) or amorphous clusters (figure 4). We considered the full-width at half-maximum of the transition region in figures 3 and 4 to estimate the radii. The asterisk marks the energy deposition value at which no defects or amorphous clusters were obtained. At higher $\mathrm{d}E/\mathrm{d}x$, the track radius increases and then shows signs of leveling off at around 4 nm. More data is needed at higher $\mathrm{d}E/\mathrm{d}x$ values to make definitive remarks about the trend in track radius. For comparison, experimental studies have shown that 10 GeV Pb irradiation results in tracks with a radius of about 2.6 nm at room temperature and 1 bar of pressure in zircon. The $\mathrm{d}E/\mathrm{d}x$ was estimated to be 21 keV nm^{-1} [6]. The track radius in Au- and Xe-irradiated SiO_2 ranges from 2.4 to 4.0 nm depending on $\mathrm{d}E/\mathrm{d}x$ and the ion mass [28]. The range of track radii observed in the present simulations covers these experimental values. The present simulations are able to reproduce the experimentally observed core–shell morphology, track radius, and density changes with track radius. At the same time, the simulations provide insights into track evolution and atomic-level details of the track structure.

Figure 7(b) shows the variation of the final number of defects and ions in amorphous clusters, referred to hereafter as amorphous ions, produced by the thermal spike (left ordinate). These numbers were averaged over the last three configurations recorded. The asterisk marks the $\mathrm{d}E/\mathrm{d}x$ value for which a track is not produced. The number of defects and amorphous ions increases steadily with increasing $\mathrm{d}E/\mathrm{d}x$. The ratio of amorphous ions to defects (right ordinate) increases with $\mathrm{d}E/\mathrm{d}x$ and levels off at about 0.55 beyond $\mathrm{d}E/\mathrm{d}x$ values of 7.65 keV nm^{-1}. This value is also consistent with the ratio calculated for displacement cascades produced by 30 keV U recoils in zircon [11]. This shows that a radiation damage morphology that is characteristic of α-recoil damage in zircon is reached for $\mathrm{d}E/\mathrm{d}x$ of 7.65 keV nm^{-1}, and higher values of energy deposition will increase the extent of the damage

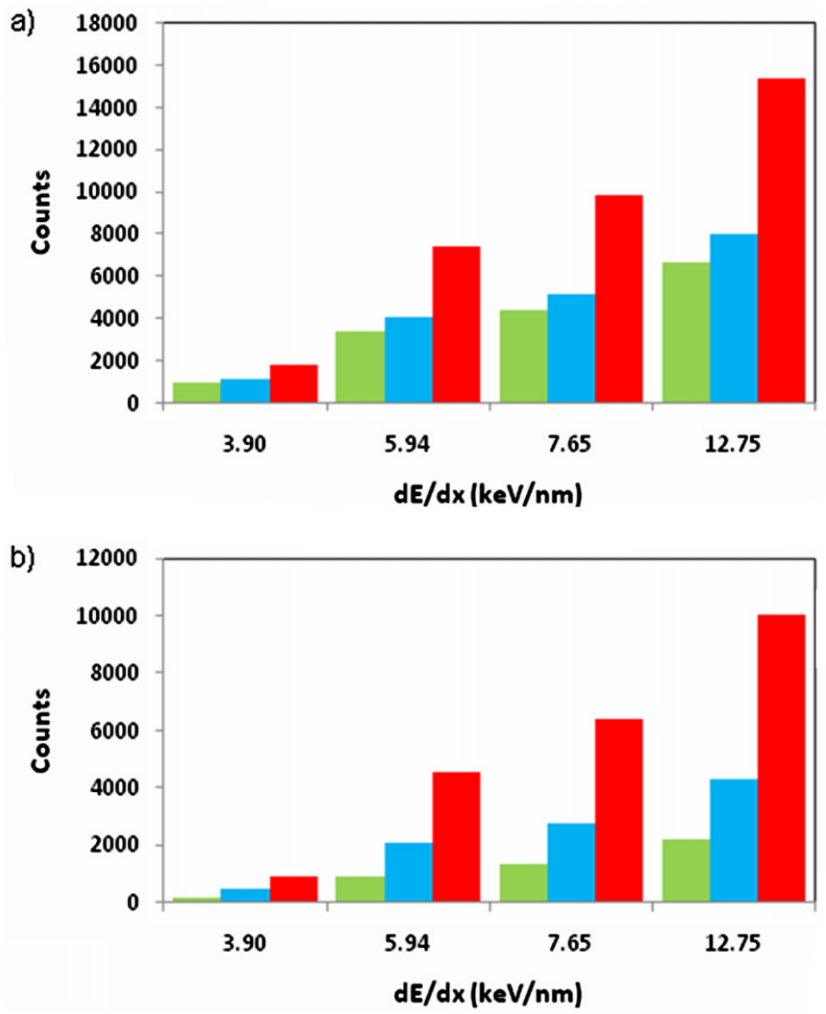

Figure 8. (a) The number of Zr (green), Si (blue) and O (red) defects as a function of $\mathrm{d}E/\mathrm{d}x$; (b) the number of amorphous Zr (green), Si (blue) and O (red) ions as a function of $\mathrm{d}E/\mathrm{d}x$.

without changing its characteristics such as the ratio of amorphous ions to defects.

The number of defects can be subdivided by species to obtain information about chemical segregation. Figure 8(a) shows the number of Zr, Si and O defects for each value of $\mathrm{d}E/\mathrm{d}x$. The values were obtained as averages over the last five configurations recorded. Defect production in fission tracks is non-stoichiometric. There is almost one anion defect for each cation defect, and the number of Si defects is 17% greater than the number of Zr defects. Explaining these differences based on displacement threshold energies (E_d) of the sublattices is difficult, because Zr and Si have almost the same E_d and O has a much lower E_d [24]. In displacement energy calculations, a single ion is given a certain amount of kinetic energy, and the minimum energy for a stable displacement to be produced on the sublattice of the ion is taken as E_d. In thermal spikes, a large number of ions are collectively energized and the excess energy dissipation mechanism may be quite different from that for the case of displacement of a single ion.

Figure 8(b) presents the relative numbers of Zr, Si and O ions in the amorphous clusters. There are about 1.5 anions for each cation. Again, the stoichiometric relation of zircon is not followed and there are more than two Si for each Zr. Atomistic simulation of collision cascades in zircon have found that the Zr coordination number in the damaged region is around six instead of eight in a perfect zircon crystal and that the displaced Si ions are polymerized, i.e. connected to each other by common O neighbors, to a degree of polymerization of 1.5. The formation of Si–O–Si networks may be a contributing factor to the small number of anion defects relative to stoichiometry. Si is more than twice as numerous as Zr in amorphous clusters, while Si is only about 17% more numerous than Zr in defects, which include amorphous clusters. Therefore, it is reasonable to conclude that the core of the track that is rich in amorphous clusters is enriched in Si, while the periphery of the track that has defective crystalline regions is relatively richer in Zr. Phase separation into Si-rich regions at the core and Zr-rich regions at the periphery of the damage has been reported in simulations of 30 keV U recoil damage in zircon [11], and this may be a characteristic feature of irradiated zircon regardless of whether it is an alpha-recoil event or swift heavy ion damage.

We have also examined the mean square displacement (MSD) of ions as a function of time and $\mathrm{d}E/\mathrm{d}x$. This data

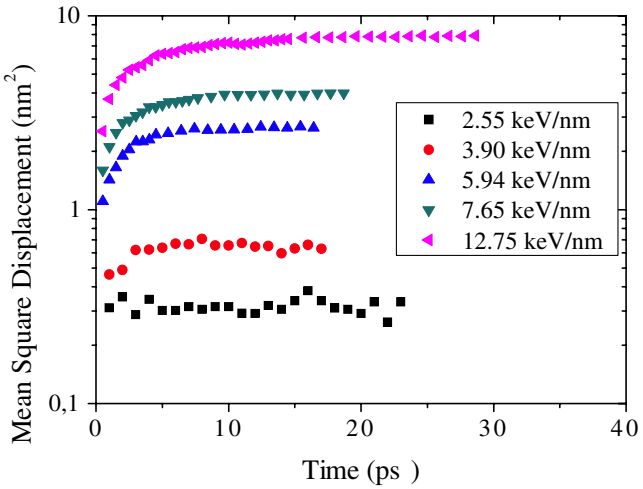

Figure 9. Mean square displacements of ions from their original site as a function of time for different values of dE/dx.

is shown in figure 9. Within the first ps, the MSD rises rapidly with time. From 1 to 5 ps, the MSD increases with time but at a slower rate. After 5 ps, the MSD becomes flat and the fission tracks become stable after about 15 ps. The great mobility of ions in the initial stage of the thermal spike indicates ballistic movement. According to MCT, the second stage of slow increase of MSD can be described by MSD being proportional to $\sim t^{\beta}$, where β is an increasing function of temperature. In this stage, due to the strong Coulombic interaction, the ions cannot exit a cage formed by their neighbors. The MSD plateau corresponds to the vibration of ions inside the cage. The present simulations have provided insights into the evolution of the fission track in zircon, the threshold dE/dx for track formation, and phase separation into a Si-rich track core and Zr-rich track periphery.

4. Conclusions

We have used molecular dynamics to simulate thermal spikes in zircon for different values of energy deposition per unit path length (dE/dx). For dE/dx below 3.9 keV nm^{-1}, the damage recovers completely and a damage track is not produced. For higher values of dE/dx, a core–shell track structure is produced with amorphous, defective and crystalline material in the core and defective crystalline material in the shell. The thermal spike produces a vigorous ballistic phase with rapid ionic motion and a decrease in core density by 28%. Ions in the core are expelled by a pressure wave into the peripheral region and then return to the core as the surrounding crystal relaxes. The final density of the core is about 6.5% less than that of crystalline zircon. As a consequence of the resulting structural rearrangement, the core becomes enriched in Si and the periphery in Zr. The overlap of tracks will lead to amorphization of the material, and nanoscale phase separation of zircon into Si- and Zr-rich regions.

Acknowledgments

This work was supported by the Materials Sciences and Engineering Division, Office of Basic Energy Sciences (BES), US Department of Energy (DOE) under Contract No. DE-AC05-76RL01830. The computations were performed using resources of the EMSL, a national scientific user facility sponsored by the DOE's Office of Biological and Environmental Research located at Pacific Northwest National Laboratory. PAFPM acknowledges CNPq (Conselho Nacional de Desenvolvimento Cientifico e Tecnologico), Brazil, for a fellowship.

References

[1] Ewing R C 1999 *Proc. Natl Acad. Sci. USA* **96** 3432
[2] Enkelmann E, Garver J I and Pavlis T L 2008 *Geology* **36** 915
[3] Zhang M, Salje E K H, Farnan I, Graeme-Barber A, Daniel P, Ewing R C, Clark A M and Leroux H 2000 *J. Phys.: Condens. Matter* **12** 1915
[4] Ewing R C, Meldrum A, Wang L M, Weber W J and Corrales L R 2003 *Rev. Miner. Geoch.* **53** 387
[5] Farnan I, Cho H and Weber W J 2007 *Nature* **445** 190
[6] Lang M, Lian J, Zhang F, Hendriks B W H, Trautmann C, Neumann R and Ewing R C 2008 *Earth Planet. Sci. Lett.* **274** 355
[7] Cavagna A 2009 *Phys. Rep.* **476** 51
[8] Morgan N A and Spera F J 2001 *Geochim. Cosmochim. Acta* **65** 4019
[9] Crocombette J P and Ghaleb D 2001 *J. Nucl. Mater.* **295** 167
[10] Trachenko K O, Dove M T and Salje E K H 2002 *Phys. Rev.* B **65** 180102
[11] Devanathan R, Corrales L R, Weber W J, Chartier A and Meis C 2006 *Mol. Simul.* **32** 1069
[12] Fleisher R L, Price P B and Walker R M 1975 *Nuclear Tracks in Solids: Principles and Applications* (Berkeley, CA: University of California Press)
[13] Bonfiglioli G, Ferro A and Mojoni A 1961 *J. Appl. Phys.* **32** 2499
[14] Szenes G 1994 *Phys. Rev.* B **51** 8026
[15] Szenes G 1995 *Phys. Rev.* B **52** 6154
[16] Bringa E M and Johnson R E 2002 *Phys. Rev. Lett.* **88** 165501
[17] Itoh N, Duffy D M, Khakshouri S and Stoneham A M 2009 *J. Phys.: Condens. Matter* **21** 474205
[18] Duffy D M and Rutherford A M 2007 *J. Phys.: Condens. Matter* **19** 016207
[19] Ismail A E, Greathouse J A, Crozier P S and Foiles S M 2010 *J. Phys.: Condens. Matter* **22** 225405
[20] Devanathan R, Durham P, Du J, Corrales L R and Bringa E M 2007 *Nucl. Instrum. Methods Phys. Res.* B **255** 172
[21] Zhang J, Lang M, Ewing R C, Devanathan R, Weber W J and Toulemonde M 2010 *J. Mater. Res.* **25** 1344
[22] Todorov I T, Smith W, Trachenko K and Dove M T 2006 *J. Mater. Chem.* **16** 1911
[23] Yu J, Devanathan R and Weber W J 2009 *J. Mater. Chem.* **19** 3923
[24] Moreira P A F P, Devanathan R, Yu J and Weber W J 2009 *Nucl. Instrum. Methods Phys. Res.* B **267** 3431
[25] Ziegler J F, Biersack J P and Littmark U 1985 *The Stopping and Range of Ions in Matter* (New York: Pergamon)
[26] Berendsen H J C, Postma J P M, van Gunsteren W F, DiNola A and Haak J R 1984 *J. Chem. Phys.* **81** 3684
[27] Humphrey W, Dalke A and Schulten K 1996 *J. Mol. Graph.* **14** 33
[28] Kluth P, Schnohr C S, Pakarinen O H, Djurabekova F, Sprouster D J, Giulian R, Ridgway M C, Byrne A P, Trautmann C, Cookson D J, Nordlund K and Toulemonde M 2008 *Phys. Rev. Lett.* **101** 175503